



Review

Recent trends in 8–14 μm type-II superlattice infrared detectorsDominic Kwan^{a,*}, Manoj Kesaria^{a,*}, Ezekiel Anyebe Anyebe^b, Diana Huffaker^{a,b,1}^a School of Physics and Astronomy, Cardiff University, The Parade, Cardiff CF24 3AA, United Kingdom^b School of Engineering, Cardiff University, The Parade, Cardiff CF24 3AA, United Kingdom

ARTICLE INFO

Keywords:

Type-II superlattice
 Long-wavelength infrared
 HgCdTe
 Carrier lifetime
 Diffusion length

ABSTRACT

Type-II superlattices (T2SLs) hold enormous potential for next-generation 8 – 14 μm long-wavelength infrared (LWIR) detectors for use at high operating temperature (HOT). The inherent flexibility of the material system has enabled the incorporation of unipolar barriers to eliminate generation-recombination currents and enhance device performance. In addition to suppressed Auger recombination and tunneling currents, this has led to sustained research interest in this material system over the past several decades. For these reasons, they are theoretically predicted to outperform the current state-of-the-art Mercury Cadmium Telluride (MCT) detectors. This review provides an overview of LWIR T2SL detectors and highlights some recent developments towards HOT applications. Recent studies on the minority carrier lifetime and diffusion length of T2SLs are examined to appraise the extent to which they limit the performance of HOT LWIR T2SL detectors. Strategies for mitigating these limitations are also explicated.

1. Introduction

Infrared photodetectors operating in the 8 – 14 μm spectral-domain are essential for several important applications including space, defense and medical imaging. For several decades Mercury Cadmium Telluride (MCT) has been the material of choice for long-wavelength infrared (LWIR) photodetection with well-established technology, high performance, and wavelength tunability. However, MCT-based LWIR detectors require cryogenic cooling which, in combination with various fabrication difficulties, has resulted in the quest for alternative material systems. The industry-driven desire for reduced size, weight and power consumption (SWaP) has led manufacturers to pursue high operating temperature (HOT) devices which negate the need for bulky cooling systems.

The Type-II InAs/GaSb Superlattice (T2SL) structure, comprised of a periodic sequence of alternating InAs and GaSb layers, which was first developed by Sai-Halasz and Esaki [1] in 1977, has emerged as a highly promising alternative to MCT. This is a result of its exceptional properties including the characteristic type-II broken gap or type-III alignment as illustrated in Fig. 1 which leads to the formation of spatially separated electrons and a holes in the InAs and GaSb layers of the quantum wells (QWs), respectively. The interactions between adjacent QWs forms a periodic potential resulting in the formation of minibands

analogous to the band structure of bulk crystals. The charge transfer, caused by the spatial separation of electrons and holes, gives rise to a local electric field and interlayer tunneling of carriers which does not need to be externally induced by an applied bias or doping. [2]

The SL bandgap is determined by the well widths and the interaction strength between adjacent QWs. Thus, by careful choice of the SL layer thicknesses, the T2SL material system becomes a narrow-gap semiconductor with a tunable bandgap. It was proposed by Smith and Mailhot [3] in 1987, that these properties could be exploited for the manufacture of T2SLs for IR detector applications. Furthermore, owing to the small lattice mismatch between the materials of the 6.1 \AA family (III-V materials with lattice constants close to 6.1 \AA), the T2SL structure provides the needed flexibility for combining different material systems enabling device designs tailored for optimal performance in optoelectronic applications. For instance, any combination of InAs, GaSb and AlSb binaries that make up the 6.1 \AA family could be utilized for an ideal superlattice application (Fig. 2). The unique properties of T2SLs have led to many suggested theoretical advances over the current state-of-the-art MCT LWIR detectors. Grein et al. [4,5] demonstrated suppression of Auger recombination by several orders of magnitude in T2SLs in comparison to MCT (this is discussed in more detail in Section 2). The flexibility provided by the 6.1 \AA family has also been used for the design and growth of innovative barrier architectures capable of mitigating

* Corresponding authors.

E-mail addresses: KwanDC@cardiff.ac.uk (D. Kwan), kesariam@cardiff.ac.uk (M. Kesaria).¹ Electrical Engineering Department, The University of Texas at Arlington, Arlington 76019, United States of America.

generation-recombination (G-R) current (see Section 3.1).

The material advantages of III-V compounds, compared to MCT which is a II-VI compound, include lower defect density, greater robustness and suppression of tunneling currents due to larger effective masses. T2SLs also hold production advantages over MCT including the “-ilities”: operability, uniformity, stability, producibility, and affordability for FPA applications while lattice-matched GaSb substrates are now available in 2”, 3”, 4” and 6” diameters. High yield for wafer growth and FPA fabrication in addition to the presence of III-V compound commercial industry is also advantageous.

The increased interest in the development of T2SL was largely stimulated by impressive results of pioneering theoretical studies in the 1970’s. In 1978, Sai-Halasz et al.[6] demonstrated that InAs/GaSb superlattices can exhibit semiconducting properties in the thinner InAs and GaSb layers. In the same year, Nucho and Madhukar[7] showed that by increasing the magnitude of the discontinuity, the superlattice bandgap changes from direct gap to indirect gap or semimetal. However, despite promising theoretical proposals, high-quality T2SL detectors were not realized experimentally until after notable advancements in molecular beam epitaxy (MBE) technology. The first experimental demonstration of InAs/Ga_{0.64}In_{0.36}Sb (38/16 Å) T2SL detector was performed by Johnson et al.[8] in 1996 with a photoresponse up to 10.6 μm realized. A year later, Mohseni et al. [9] demonstrated MBE growth and characterization of InAs/GaSb T2SL for LWIR detectors. In the same year, LWIR photodetection was demonstrated by Fuchs et al.[10] using an InAs/GaInSb T2SL with significant suppression of band-to-band tunneling currents coupled with improvement in material quality. A significant milestone was reached in 2004[11] with the first development of a high performance T2SL focal plane array (FPA) which confirmed the aptitude of the T2SL material system for IR photodetection (a more detailed survey of the recent developments in LWIR T2SLs is given in Section 4).

The past decade has seen the development of Ga-free (usually InAs/InAsSb) T2SL detectors as a possible alternative to the more well-established Ga-containing (usually InAs/GaSb) variant. The Ga-free T2SL was first proposed as an InAs_{0.4}Sb_{0.6}/InAs_{1-x}Sb_x strained-layer

superlattice, with $x > 0.6$ for LWIR detector applications, by Osbourn in 1984.[12] The authors used the strain and type-II band alignment of the InAsSb/InAsSb material system to reduce the bandgap below what was achievable at the time through bulk semiconductors. Growth and fabrication of Ga-free T2SLs were demonstrated throughout the 1990’s with notable developments including the InAsSb/InSb SLS LWIR detector grown by Metalorganic Chemical Vapor Deposition (MOCVD), [13] InAs/InAsSb T2SLs LEDs on GaAs substrates[14–16] and InAs/InAsSb T2SL lasers on InAs substrates.[17,18] However, interest in LWIR Ga-free T2SLs waned until around 2011[19] when it was reported they exhibit significantly longer minority carrier lifetime in comparison to their Ga-based counterpart[20] coupled with renewed interest from several research groups, notably Arizona State University (ASU), [20–25] the Centre for Quantum Devices at Northwestern University (CQD)[26–28] and the NASA Jet Propulsion Lab.[29–31] Both Ga-containing and Ga-free T2SLs continue to be pursued for LWIR detectors with both material systems exhibiting clear advantages and disadvantages.

In addition to longer minority carrier lifetimes, a notable advantage of the Ga-free material system for LWIR detectors is its tolerance to defects. This arises from the very low lying defect states in resonance with the conduction band instead of the bandgap.[24,32] This defect tolerance is particularly advantageous for the heteroepitaxy on lattice-mismatched substrates such as GaAs.[33] The surface of the Ga-free T2SL is inherently n-type which is advantageous for n-type absorber regions in which surface band bending will repel minority carriers and reduce surface current. However, this same effect will be problematic for p-type absorbers.[34] The growth of Ga-free T2SLs is also thought to be more straight forward due to the availability of a simple shutter sequence in which only the Sb shutter is switched on and off. This contrasts with Ga-containing T2SLs in which four shutters must be carefully controlled and the problem of interfaces and strain balancing addressed. However, some groups have employed more complex shutter sequences for the growth of Ga-free T2SLs using two Sb shutters for better control of Sb content.[35] Nevertheless, the Ga-containing T2SL holds two major advantages over the Ga-free in the LWIR spectral range.

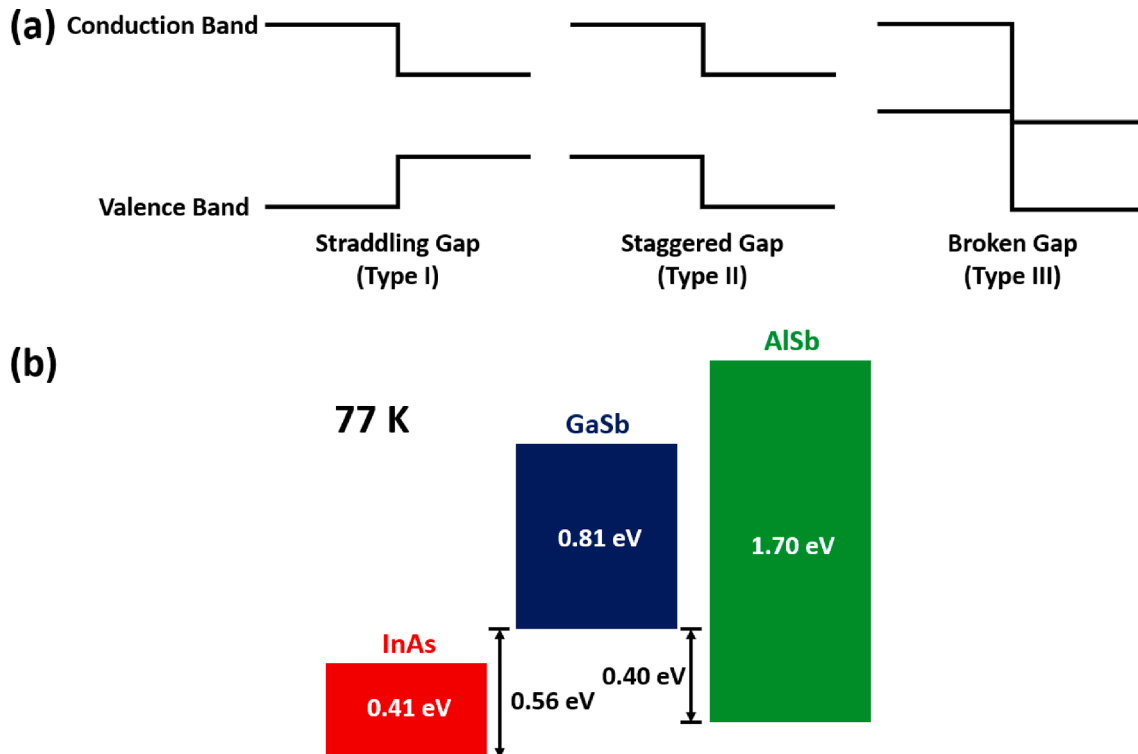


Fig. 1. (a) Heterostructure band alignment types (b) The band alignment of the 6.1 Å family of semiconductors.

Firstly, the Ga-containing T2SL requires a significantly shorter period thickness compared to the Ga-free to reach the same cut-off wavelength. The shorter period of the Ga-containing T2SL results in stronger oscillator strength and thus stronger absorption, particularly in the LWIR spectral range. Secondly, while both material systems have comparable electron effective masses, the hole effective mass of the Ga-free T2SL is notably larger than the Ga-containing resulting in unfavorable hole transport properties.[29] This issue also worsens for longer wavelength and lower Sb content, making it particularly problematic for LWIR detectors. By contrast, due to the position of the heavy hole mini band in the broken gap, the hole transport properties of the Ga-containing T2SL have a very weak dependence on the cut-off wavelength. Considering these findings, no one material system has demonstrated an overall advantage over the other and so both are widely pursued LWIR detectors.

The majority of LWIR detectors are designed for space and defense applications meaning the reduction of the size, weight and power consumption (SWaP) is a foremost consideration. Unfortunately, the SWaP of modern LWIR detector modules is undermined by the bulky cooling systems required for low-temperature and high-performance operation. The theoretical advantages of the LWIR T2SL detectors have led to much expectation that this material could form the basis for the next generation of HOT, low SWaP LWIR detectors. Considering recent experimental findings and theoretical modelling, some of which challenges long-established conceptions of T2SL physics, it is necessary to reappraise the prospects of LWIR T2SL photodetectors. This paper systematically reviews recent developments in the structure and performance of LWIR photodetector devices while highlighting novel avenues for improving device performance and increasing operating temperature.

2. Figures of merit

The figures of merit, described in this section, are powerful tools for accurately appraising and comparing the performance of LWIR detectors.[36]

2.1. Quantum efficiency

The External Quantum Efficiency (EQE) of a photodetector is defined as the number of carriers measured at the detector output divided by the flux of incident photons and is given by:

$$\eta = \frac{I_{ph}}{q\Phi A_d} \quad (2.1)$$

where I_{ph} is the photocurrent, q is the electron charge, Φ is the photon incidence and A_d is the effective optical area of the detector. Thus, the EQE is less than 1 but usually given as a percentage.

2.2. Responsivity

The external quantum efficiency defined above is closely related to the responsivity which relates the output signal of a detector (in Amps or Volts) to the radiant input that produced that signal (in Watts) and is given by:

$$R = \frac{\eta q}{h\nu} \quad (2.2)$$

where $h\nu$ is the energy of incident photons. The spectral responsivity gives the responsivity in terms of wavelength while the blackbody responsivity gives the peak responsivity.

2.3. Noise equivalent power

The signal-to-noise ratio (SNR) is described by the following equation:

$$SNR = \frac{R\phi_e}{i_n} \quad (2.3)$$

where ϕ_e is the radiant power and i_n is the noise expressed as current. The noise equivalent power (NEP) is a measure of the incident radiant power, its unit is Watts and produces an SNR of unity given by:

$$NEP = \frac{i_n}{R} = \frac{\phi_e}{i_{signal}/i_{noise}} \quad (2.4)$$

The lower the NEP, the more sensitive the device, although it does not allow direct comparison between different detector configurations.

2.4. Specific detectivity

To compare detectors in any given configuration, the specific detectivity is the inverse of the NEP which take into accounts both the active area and the signal bandwidth of the detector. It represents the primary figure of merit for comparing IR detectors and is given by:

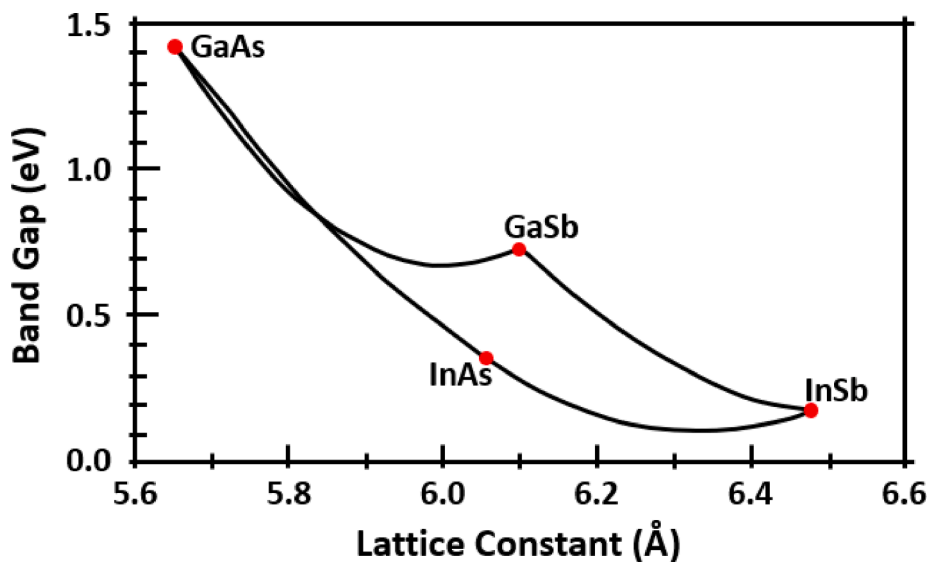


Fig. 2. The band energy and lattice constant of various compound semiconductor binaries.

$$D^* = \frac{\sqrt{A_d \Delta f}}{NEP} \quad (2.5)$$

where Δf is the signal bandwidth. It can thus be seen that the major figures of merit for IR detectors are determined by the signal-to-noise ratio, where the signal is related to the EQE, and the noise, which is related to the dark current.

2.5. Dark current

The dark current is the current flowing through the detector in the absence of any incident photon flux. Through the use of modelling based on experimental data, Gopal et al.[37–39] have identified that the diffusion current, generation-recombination current (G-R), trap-assisted tunneling current (TAT) and ohmic shunt current are the main sources of dark current in a T2SL. The diffusion of minority carriers from high to low concentrations is the diffusion current modelled as:

$$I_{diff} = \frac{qAn_i^2}{N_d} \left\{ \frac{kT}{q} \frac{\mu_h}{\tau_h} \right\}^{1/2} \tanh \frac{d}{L_h} \left[\exp \left(\frac{qV}{kT} \right) - 1 \right] \quad (2.6)$$

where A is the junction area, n_i is the intrinsic carrier concentration, N_d is the donor concentration, μ_h is the hole mobility, τ_h is the hole lifetime, V is the diode bias voltage, d is the thickness of the n region, and L_h is the hole diffusion length.

G-R current is generated due to depletion region defects which act as Shockley-Read-Hall (SRH) recombination centers. For reverse bias, considered above, the G-R current can be given by:

$$I_{G-R} = \frac{qAn_i W_{dep} V}{V_i \tau_{G-R}} \quad (2.7)$$

$$A_{G-R} = \frac{qn_i A}{2\tau_{G-R}} \left[\frac{2\epsilon_0 \epsilon_s (N_a + N_d)}{qN_a N_d} \right]^{1/2} \quad (2.8)$$

where τ_{G-R} is the G-R lifetime, N_a is the acceptor concentration and W_{dep} is the depletion region width. The TAT current originates from mid-gap

trap states, which carriers can use to tunnel between bands, usually under a high electric field, and is expressed as:

$$I_{TAT} = \frac{\pi^2 q^2 A m_e V_r M^2 N_T}{h^3 (E_g - E_t)} \times \exp \left\{ - \frac{8\pi(2m_e)^{1/2} (E_g - E_t)^{3/2}}{[3qhF(V)]} \right\} \quad (2.9)$$

where m_e is the effective mass related to the tunneling, E_g is the T2SL bandgap, E_t is the trap energy level below the conduction band edge, h is Planck's constant, M is the matrix element of the trap potential, N_T is the trap density, $F(V)$ is electric field strength across the depletion region which is dependent on voltage.

Ohmic shunt currents are usually caused by native oxides, formed on the mesa sidewalls during etching, which act as good conductors. This component can simply be described using Ohm's law:

$$I_{sh} = \frac{V}{R_{sh}} \quad (2.10)$$

where R_{sh} is the diode shunt resistance. An understanding of which dark current mechanism is dominant for a given voltage or temperature is essential for improving device performance.

3. Performance comparison of MCT and T2SL

3.1. Dark current

The theoretical advantages of T2SL detectors over MCT is yet to be experimentally demonstrated in superior device performance. Fig. 3 shows that the state-of-the-art T2SL LWIR detectors have dark currents approximately within one order of magnitude of Rule 07 (which provides a heuristic predictor for the state-of-the-art performance of an MCT photodiode).[40] The dark current of devices fabricated by various research groups including the Centre for Quantum Devices, (CQD) Northwestern University, USA,[35,41] Semiconductor devices (SCD) Israel,[42] Jet propulsion Laboratory (JPL) at the National Aeronautics and Space Administration (NASA), USA,[43,44] Shanghai Institute of

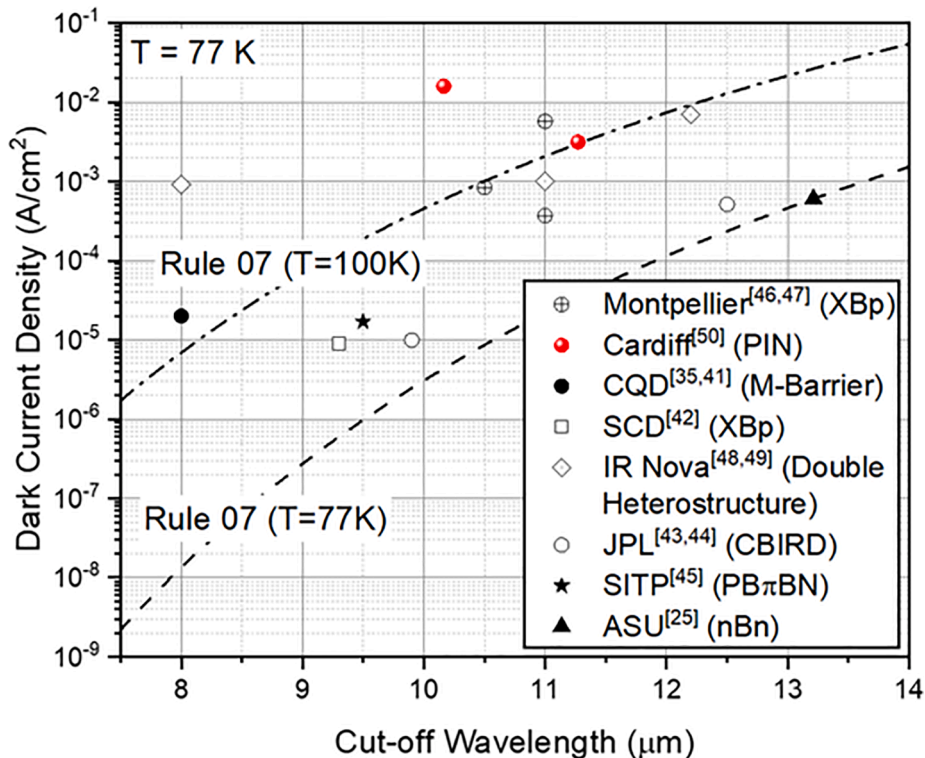


Fig. 3. Collected values of the dark current density at 77 K for long-wavelength infrared type-II superlattice detectors compared with 'Rule 07' for HgCdTe Detectors.

Technical Physics (SITP) of the Chinese Academy of Sciences, China, [45] Arizona State University (ASU), USA, [25] Institut d'Électronique et des Systèmes, France, [46,47] IRnova AB, Sweden, [48,49] and Cardiff University, Wales [50] have been compared. The performance of T2SLs only becomes competitive with MCT when cooled to lower temperatures.

The dark current at low reverse bias is limited by the G-R current at low temperatures and the diffusion current at higher temperatures (Fig. 3). Equations (2.6) and (2.7) show the dark current is strongly inversely dependent on the minority carrier lifetime and diffusion length. Because of the short minority carrier lifetimes, particularly for Ga-containing, and diffusion lengths of T2SLs it is inferred that these are the parameters limiting T2SLs from outperforming MCT.

3.2. Diffusion length in LWIR T2SLs

In addition to its contribution to the dark current, the minority carrier diffusion length also affects the performance of LWIR T2SLs through the collection efficiency. It is generally understood that to achieve high quantum efficiencies, the active region thickness of a detector should be equal to, if not greater than, the target cut-off wavelength. However, increasing the active region thickness larger than the diffusion length might not yield the desired increase in device performance. This is because carriers generated within the region larger than the diffusion length from the contact are unlikely to be collected. Klipstein et al. [51] have reported minority carrier diffusion lengths for T2SLs in the range of 3 – 7 μm at 78 K using k.p simulations fit to experimental data. As a result, T2SL active region thicknesses have been limited to around 6 μm to maintain high collection efficiencies of around 90%. To extend the active region thickness into the range desirable for LWIR applications ($\sim 10 \mu\text{m}$) to increase absorption would significantly affect the collection efficiency. Furthermore, critical thickness issues arising from the internal strain of the superlattice can cause a degradation of material quality with an increase in the thickness of the

constituent layers of the superlattice. This issue arises from the slight lattice mismatch between InAs and GaSb (or $\text{InAs}_x\text{Sb}_{1-x}$). As more layers of a non-lattice matched material are deposited on another, the internal strain energy in the structure increases. This energy will continue to increase until a certain critical thickness is reached beyond which the formation of dislocations becomes energetically favourable. The Matthews Blakeslee model [52] provides a generalised formula for the critical thickness for a given combination of two materials. The diffusion length for MCT has been reported to be around 20 μm meaning there is no trade-off between absorption and collection efficiency. As a result, as Fig. 4 highlights, MCT detectors can capitalize on longer diffusion lengths and achieve higher QEs using thicker active regions.

The EQE of devices from Montpellier, [46,47] JPL, [44] SITP, [45] IR Nova AB, [49,53] SCD, [54] Aim Infrarot-Module (AIM) GmbH, [55–57] Germany and ASELSAN AS, [58] Turkey are compared in Fig. 4. The clear advantage of MCT, arising from the diffusion length, is not necessarily maintained as the temperature increases above 77 K. The literature contains somewhat conflicting arguments regarding the temperature dependence of the minority carrier diffusion length. Some have assumed that the diffusion length decreases at higher temperatures, [59] possibly due to the reduction in minority carrier lifetime suggested by the known $T^{-1/2}$ dependence of SRH lifetimes (this will be discussed in more detail below). However, recent reports suggest otherwise. Klipstein et al. [51] reported that in T2SL over the temperature range 70 – 130 K, the lateral diffusion length varies linearly with an increase in temperature from 6.3 μm (78 K) to 11 μm (130 K). These findings are also in agreement with diffusion coefficient dependence on the temperature which is described by:

$$D = \frac{kT}{e} \mu \quad (3.1)$$

where D is the diffusion coefficient, k is the Boltzmann constant, T is the temperature and μ is the mobility. Note, however, that it is the vertical diffusion length, not the lateral diffusion length, that limits detector

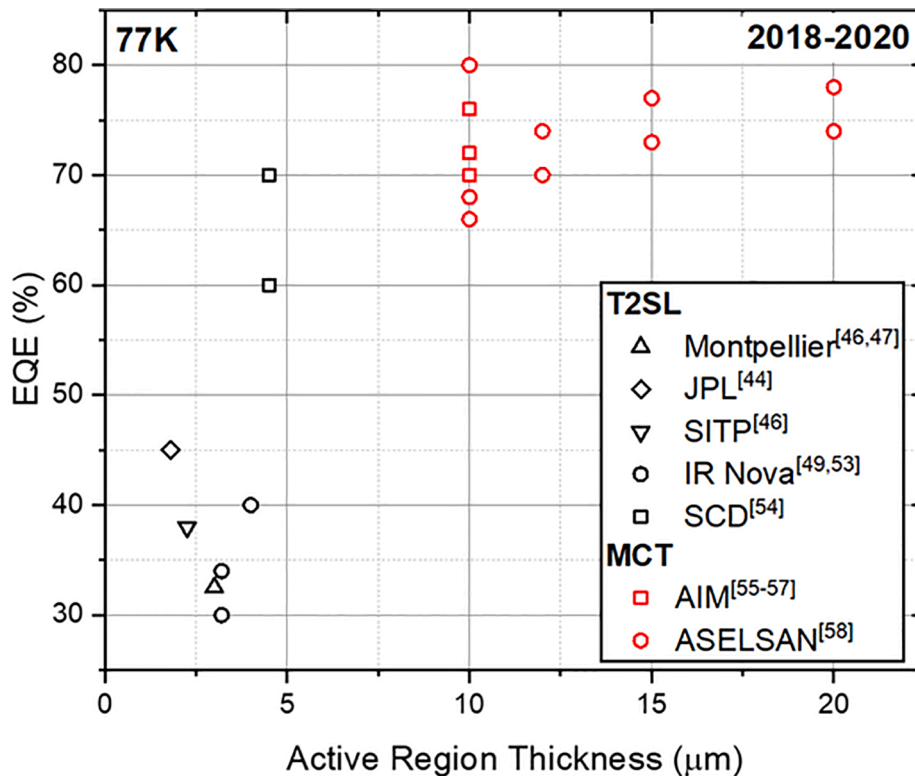


Fig. 4. Collected values of external quantum efficiency vs active region thickness for recent (2018–2020) superlattice-based and HgCdTe-based long-wavelength infrared detectors.

performance and it is not possible to measure the vertical diffusion length in this way. Furthermore, Taghipour et al.[60] directly measured the vertical diffusion length of InAs/GaSb T2SLs at temperatures from 80 to 170 K using the Electron-Beam Induced Current (EBIC) method. The preponderance of the findings suggest that the vertical diffusion length stays constant at around 1.5 μm for the temperature range 80 – 140 K and increases roughly linearly to 4.5 μm at 170 K. However, data from low e-beam energy (~ 10 keV) shows a linear relationship from 80 K. These studies suggest that the diffusion length of T2SLs increases with temperature even up to ~ 11 μm at 130 K. If this is the case, the advantage of MCT, whereby thicker active regions are used to obtain higher quantum efficiencies, will be eroded at higher temperatures. With a diffusion length comparable to the intended cut-off wavelength, HOT LWIR T2SL detectors could employ sufficiently thick active regions with no loss of collection efficiency, provided issues related to critical thickness can be overcome. Furthermore, the critical thickness issues that inhibit the growth of thick, high-quality T2SL material may not be as detrimental as first thought. This is because Klipstein et al. have reported that the vertical diffusion length, which contributes to device performance, may be less affected by degradations in material quality than lateral diffusion lengths.

3.3. Minority carrier lifetime

The minority carrier lifetime contributes to the dark current of T2SL detectors as expressed by Equations (2.3) and (2.4) as well as the detectivity and operating temperature. It is linked to the diffusion length by:

$$L = \sqrt{D}\tau \quad (3.2)$$

where L is the minority carrier diffusion length and τ is the minority carrier lifetime. As shown in Fig. 5, the typical lifetimes for LWIR SLs are in the range of 10–30 ns for Ga-containing and 100–400 ns for Ga-free T2SLs. This increases to around 100 ns and 2–10 μs respectively for the MWIR spectral range.

The minority carrier lifetimes of T2SLs and MCT, as reported by selected research groups including Stony Brook University (SBU) and U. S. Army Research Laboratory (ARL),[61–65] St. Petersburg State Polytechnical University (StP),[62] JPL,[66,67] Arizona State University (ASU),[20,25] Sadia National Laboratories (SNL),[68,69] University of Iowa (U Iowa),[69] Cardiff University,[50] U.S. Army Night Vision and Electronic Sensors Directorate (NVESD),[70] DRS Infrared Technologies

[now Leonardo DRS] (DRS)[71] and SRI International[72] are compared in Fig. 5 which also shows a near-linear decrease in carrier lifetime with increasing wavelength for both Ga-containing and Ga-free. It also highlights the limitation posed by minority carrier lifetime in LWIR T2SLs. However, Ga-free T2SLs have lifetimes comparable to MCT in the MWIR range and the LWIR lifetimes are in the proximity of an order of magnitude to that of MCT. As the lifetime directly affects the diffusion current of T2SL devices according to $I_{\text{diff}} \sim \tau^{-1}$, the performance of diffusion-limited Ga-free T2SL devices is expected to greatly exceed that of Ga-containing detectors, however, this has not yet been realized. For a detailed analysis of T2SL lifetimes and their effect on device performance, the reader is directed to the following reviews. [59,73]

The minority carrier lifetime in a T2SL is a combination of Shockley Read Hall (SRH), Auger and radiative recombination processes where:

$$\tau^{-1} = \tau_{\text{SRH}}^{-1} + \tau_{\text{Rad}}^{-1} + \tau_{\text{Auger}}^{-1} \quad (3.3)$$

Grein et al.[4,5] have argued that the Auger contribution can be neglected in p-type T2SLs since the degeneracy split occurs in the light hole and the heavy hole by the strain in the minibands. This degeneracy, brought about by the lattice mismatch between the SL constituent materials, introduces sub bandgaps in the band structure which reduce the available phase space for Auger processes. Though this is not the case for n-type T2SLs, suppression of Auger processes can still be achieved by increasing the (In)GaSb thickness, thus flattening the lowest conduction band. However, the performance expectations set by Auger suppression is yet to be realized in T2SL devices. Since the publication of Rogalski's reviews, new research has been conducted that challenges the widely accepted physics affecting carrier lifetimes in T2SLs. Contrary to Grein's assertions, 8 band k.p modelling recently performed by Klipstein et al. [74] for an LWIR InAs/GaSb T2SL suggests that the Auger 7 (A7) process should be quite effective. The apparent dominance of the SRH process, despite the presence of an effective A7 process, suggests the physics of this area requires further study. While this may simply be explained by an unusually high concentration of Ga-related defects acting as SRH centers, the authors propose that SRH recombination and the suppression of A7 processes is caused by the concentration of donor-like traps. The latter theory is consistent with experimental data suggesting Auger rates are significantly stronger in Ga-free T2SLs compared to Ga-containing.[75]

The complex physics surrounding the recombination processes and their relative prominence in T2SLs are directly relevant for HOT device

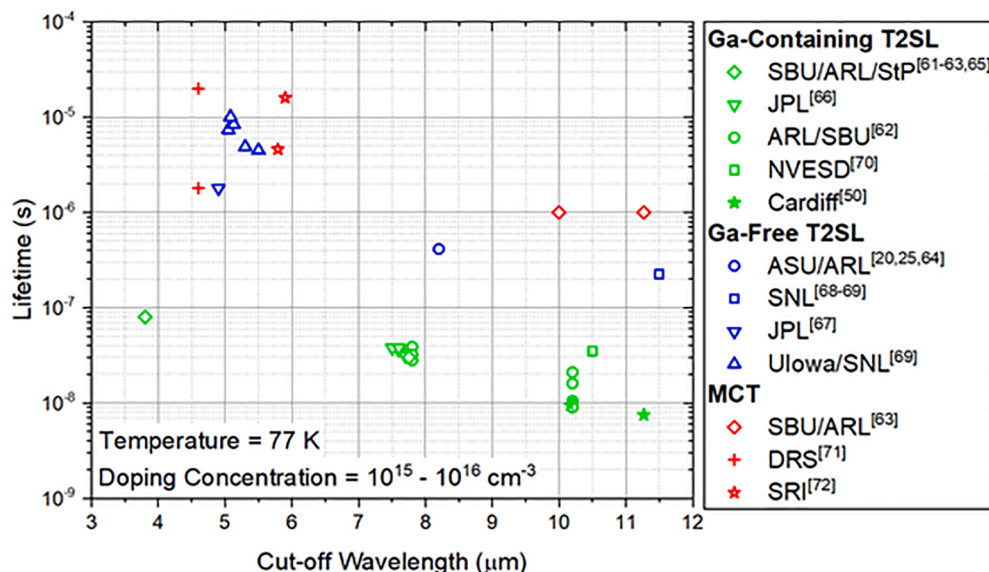


Fig. 5. Collected minority carrier lifetimes vs cut of wavelength for Ga-free and Ga-containing type-II superlattices and HgCdTe.

performance as they determine the minority carrier lifetime and its temperature dependence. Aytac et al. [75] have performed temperature-dependent measurements of recombination rates in InAs/InAsSb T2SLs and fitted the data to the theoretical behavior of SRH, radiative and Auger recombination processes. It was found that for unintentionally doped T2SLs, the SRH process dominates for the temperature range 77–200 K, during which the lifetime is roughly constant with temperature, and Auger processes dominate between 200 K to room temperature, in which the lifetime decreases with temperature. It was observed that SRH lifetimes could be increased by increasing Sb content while reducing SL period thickness, thereby reducing the number of available SRH recombination centers. Increasing Sb content was also found to reduce Auger coefficients, possibly due to conduction band flattening, though these remain much larger than for the equivalent Ga-containing T2SLs. [61] Using a similar approach Taghipour et al. [60] measured the temperature dependence of recombination mechanisms in InAs/GaSb T2SLs and found that the lifetime is SRH limited from 80 to 150 K and Auger limited above 150 K. The prevalence of Auger recombination over SRH is likely due to the relatively high ($\sim 5.0 \times 10^{16} \text{ cm}^{-3}$) doping concentration. Unlike the Ga-free T2SLs reported previously, the minority carrier lifetime of the Ga-containing T2SLs appears roughly constant with temperature over a range of 80 K to room temperature. More experimental studies are required to understand the recombination mechanisms in T2SLs, it can be concluded based on the current research that the minority carrier lifetime remains roughly constant as the temperature is increased.

These results suggest that the material limitations of the T2SL, namely the minority carrier diffusion length and lifetime, does not deteriorate with an increase in the operating temperature from 77 K to around 150 K for both Ga-containing and Ga-free T2SLs.

4. Strategies for improved performance of LWIR T2SL detectors

Despite the limitations to device performance described in Section 2, interest in the T2SL material system remains strong with ongoing developments towards the realization of HOT LWIR T2SL detectors. This section provides a sampling of these developments.

4.1. Barrier infrared detectors

The development of the T2SL nBn detector by Maimon and Wicks in 2006 [76] represents a major advancement in T2SL capability. The nBn device (Fig. 6) consists of a thin n-type region, a wide bandgap, unipolar barrier layer presenting a barrier for electrons but not holes and an n-type absorber layer. This structure has the effect of blocking the majority carrier current between the two contacts while the minority carrier

current can flow freely. These devices have lower generation-recombination and surface leakage currents giving them an edge over conventional PIN structures. The concept of the nBn has been demonstrated in LWIR T2SLs, [77] as well as several notable variations such as the pBp, [78] pBn, [79] p- π -M-n, [80] pBiBn, [81] and CBIRD. [44] In addition to the reduced dark current through suppression of G-R current, the advantages of barrier infrared detectors (BIRD) include reduced surface leakage, ease of passivation and greater tolerance to dislocations. These advantages enable BIRDs to operate at higher temperatures than conventional PIN diodes with comparable performance.

4.2. Cascade infrared detectors

As reported in Section 2.2, the diffusion length and active region thickness of T2SL LWIR detectors often impede device performance via the collection efficiency. This can worsen at high temperature as the absorption depth of LWIR radiation increases beyond the diffusion length. Cascade Infrared Detectors (CID), in which multiple absorption regions are used in sequence, are designed to mitigate this limitation. The device architecture, shown in Fig. 7, consists of two or more individual absorber regions connected by electron and hole barriers. By designing each absorber region to be thinner than the diffusion length, one can ensure that photogenerated carriers travel only to the subsequent stage where they recombine. Thus, multiple absorber layers can be grown in sequence with a combined thickness greater than the diffusion length achieving greater detectivities than observed in conventional devices. [82] A LWIR CID with an InAs/GaSb T2SL absorber region reported by Lei et al. [83] has a measured detectivity two times higher than a comparable MCT detector operating at 300 K. Please refer to the recent review reported by Hackiewicz et al. for more detail on CIDs. [84]

4.3. Modified fabrication process

When the mesa sidewalls of a T2SL are exposed by etching, oxygen diffuses to the surface and forms native oxides through the following processes: $2\text{InAs} + 3\text{O}_2 \rightarrow \text{In}_2\text{O}_3 + \text{As}_2\text{O}_3$, $2\text{GaSb} + 3\text{O}_2 \rightarrow \text{Ga}_2\text{O}_3 + \text{Sb}_2\text{O}_3$, and $\text{In}_2\text{O}_3 + \text{As}_2\text{O}_3 \rightarrow 2\text{InAsO}_3$. Not only do these oxidation processes occur readily but the resulting native oxides are good conductors leading to a problematic surface dark current. This problem is particularly challenging for (V)LWIR detectors due to the reduced bandgap for such detectors. A common solution is to physically shield the mesa sidewalls from ambient air using polyimide passivation such as SU8. [85,86] The primary advantage of this technique is its accessibility rather than its efficacy as it is widely agreed that chemical passivation is a more effective solution than physical protection from ambient air. Recently, Al_2O_3 , deposited by Atomic Layer Deposition (ALD), has been proposed as an effective form of passivation due to its favorable Gibbs free energy leading to the preferential formation of Al_2O_3 over In, Ga, As and Sb oxides. Specht et al. [87] have demonstrated that in p-type InAs/GaSb LWIR T2SLs Al_2O_3 passivation reduces the dark current by an order of magnitude. Perimeter/area analysis indicates the reduction in the surface-related component of the dark current. Furthermore, Salihoglu et al. [88,89] have demonstrated that Al_2O_3 passivation is more effective for MWIR InAs/GaSb T2SLs than conventional approaches including SiO_2 , TiO_2 , HfO_2 , ZnO , and Si_3N_4 , by several orders of magnitude in some cases. Epitaxial overgrowth of a wide-bandgap material has also been proven to be an effective method of suppressing surface leakage current. [90,91] The efficacy of this technique in T2SL arises from the large band offset between the absorber and wide-bandgap semiconductor leading to a depletion of carriers in the vicinity of the IF. An advantage of this technique over dielectric deposition is that, by doping the wide-bandgap region, the common Fermi level between the two materials can be tuned. Sulfur-based passivation, in which a covalently bonded sulfur layer passivates the outer group-III and group-V atoms, has also been proven as an effective means of

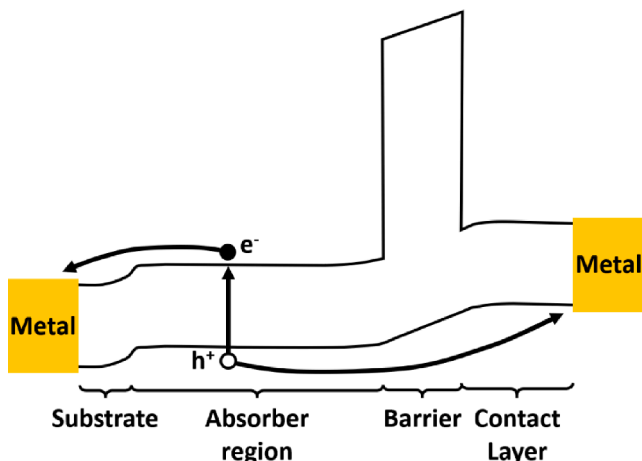


Fig. 6. Band diagram of an nBn device structure.

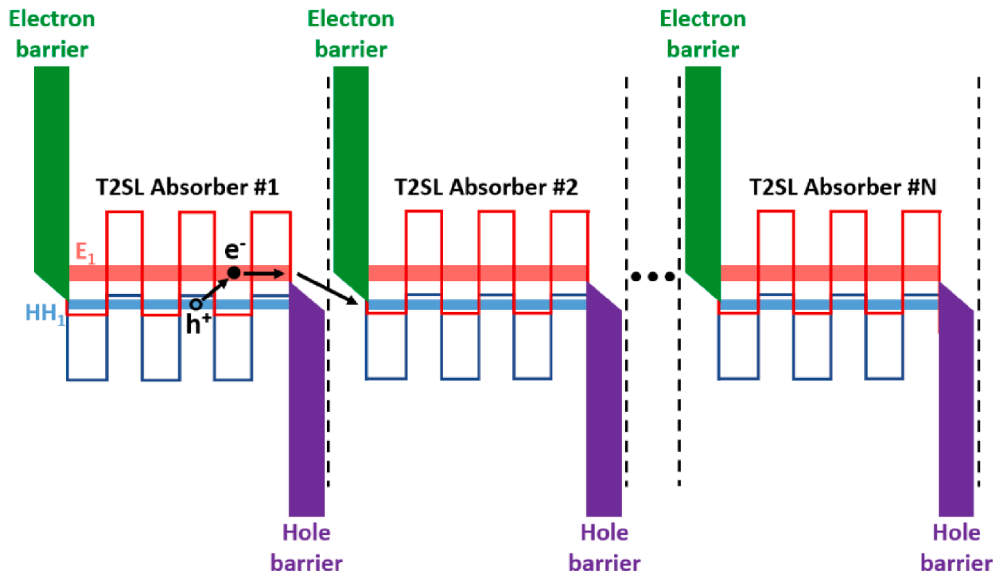


Fig. 7. Schematic of a type-II superlattice interband cascade infrared detector with N stages.

passivation and is often used in combination with a dielectric layer. [91,92] Reticulated Shallow Etch Mesa Isolation (RSEMI) and heterostructure designs are being exploited as an alternative to the chemical passivation to suppress the surface leakage current. [93,94] This approach takes advantage of the barrier architectures such as the nBn in which only the n-top contact is etched. Etching through the barrier layer of such a device would be sufficient for pixel isolation. In this way, the unetched absorber region does not contribute to the surface current. Thus far, the best passivation results for LWIR T2SLs have been achieved using the gating technique in which a metal-insulator-semiconductor (MIS) structure is deposited on the mesa sidewalls. By applying a known bias to the MIS, the surface leakage current can be effectively controlled. [95] Chen et al. [96] pioneered in reporting a two orders of magnitude reduction in the dark current using the gating technique in LWIR T2SLs by utilizing a SiO_2 passivation layer. The gating technique has now been demonstrated for LWIR T2SLs using Y_2O_3 , [97] hybrid $\text{SiO}_2\text{-Y}_2\text{O}_3$ [98] and Si_3N_4 [99] passivation layers. The major drawback of this technique is the high gate bias required for effective leakage suppression which is problematic for small-pixel FPAs although, a gated bias as low as -4.5 V has been achieved. Despite the efficacy of the gating technique and the successful demonstration of passivation using various approaches, it is surprising that there are very few reports in which these techniques have been combined. This is most likely due to the specific fabrication capabilities of individual groups however a combined approach represents a promising path to effective surface leakage suppression.

4.4. Resonator pixel (JPL)

As discussed in Section 2, the critical thickness related challenge arising from internal strain limits the thickness of T2SL absorber regions which undermines the QE. To improve QE without the need for thicker active regions, novel device designs termed resonator pixels have been proposed. In conventional detector geometry, shown in Fig. 8(a), radiation enters through the substrate and reflects between the metal reflector and the substrate/air interface resulting in the formation of a Fabry-Perot Etalon (FPE). In such a device, the transmission of the substrate/air interface is usually large enough to prevent effective confinement of photons in the active region. Furthermore, optical interference will result in an oscillating QE signature centered around the classical value. In resonator pixel design (Fig. 8(b)), sub-wavelength diffractive elements diffract the incident light. If the angle of diffraction $>$ critical angle ($\sim 16^\circ$ for GaSb) at the substrate/air interface the light will undergo total internal reflection (TIR) resulting in much greater photon confinement. By carefully adjusting the detector size and shape, one can ensure TIR occurs at the detector sidewalls and the optical path interferes constructively with itself. For a $1.8 \mu\text{m}$ thick active region and a wavelength range of $12 - 16 \mu\text{m}$, the resonator pixel design achieved a QE of 40% to 50% compared to 34.6% for the conventional design. [44]

4.5. GaAs immersion lens

It is well known that a possible path towards higher performance, room temperature operation for the LWIR detectors is by facilitating an apparent “optical” size which can be achieved using a hemispherical

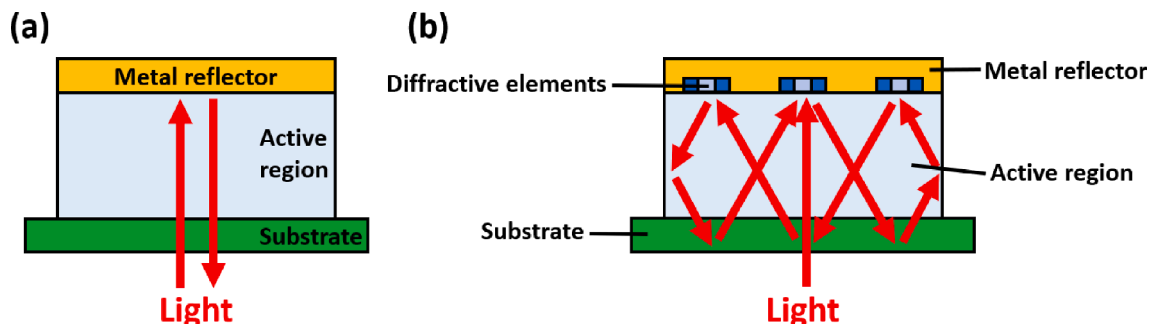


Fig. 8. Schematic of (a) optical path in conventional detector architectures and (b) optical path in resonator pixel structures.

immersion lens that concentrates the impinging IR radiation onto the detector element.[100,101] Several challenges, such as lattice matching between detector and lens material as well as transmission and reflection losses, must be addressed before optically immersed LWIR detectors can be realized. Recently, GaAs has emerged as a viable material for optically immersed HOT LWIR detectors.[33,102,103] The problem of lattice matching GaAs ($a = 5.7 \text{ \AA}$) to GaSb ($a = 6.1 \text{ \AA}$) has been effectively addressed by the Interfacial Misfit Array (IMF) technique, developed by Huffaker's group, in which a 2D array of periodic 90° dislocations are used to prevent the spread of threading dislocations.[104] The IMF technique has been demonstrated to enable the growth of high-quality LWIR T2SLs on GaAs substrates.[105] Michalczewski et al. [33,94] have reported epitaxy and fabrication of InAs/InAsSb T2SL detectors operating at cut-off wavelengths of $10 \mu\text{m}$ (LWIR) and $15 \mu\text{m}$ (VLWIR) using GaAs immersion lens technology. The IMF technique was also used to grow high quality GaSb buffer layer, $\sim 1 \mu\text{m}$ thick, on a $2''$ GaAs substrate.[106] Lattice matched InAs/InAsSb T2SLs were then grown on the GaSb buffer layer. As mentioned in Section 1, the InAs/InAsSb T2SL is an ideal choice for growth on non-lattice matched substrates due to its inherent defect tolerant properties. Following standard photolithography processing, a numerically controlled micromachined GaAs substrate is converted into an immersion lens. The detectivity at 210 K was 2×10^{10} Jones and 1.7×10^9 Jones for the LWIR and VLWIR T2SLs respectively. This is higher than commercially available MCT operating at an equivalent temperature and wavelength range by a factor of 2. Müller et al. [103] have demonstrated a similar optically immersed LWIR T2SL detector using a Ga-based absorber. A linearly graded metamorphic buffer layer was used instead of an IMF array. Using the hyper hemispherical GaAs immersion lens, a spectral detectivity of 6×10^9 Jones was achieved at 195 K , approaching the performance of MCT.

4.6. Layer thicknesses

Despite the flexibility of InAs/GaSb T2SL LWIR detectors, most of the structures reported in the literature use an SL absorption region period

of $X \text{ ML InAs}$ and 7 ML GaSb (where $X = 13$ to 15). Our group has performed extensive 8 band k.p simulations to determine the electro-optical properties of several SL structures with a predicted cut-off wavelength in the LWIR spectral range, as shown in Fig. 9.[50] The simulations highlighted SL structures, such as the 12/4 T2SL, are predicted to have superior optical properties than the conventional 14 ML InAs/7 ML GaSb T2SL. Simulations confirmed the existing hypothesis that reducing the SL period will result in a larger wavefunction overlap and, correspondingly, a larger absorption coefficient. Four reference samples with structure $X \text{ ML InAs} / Y \text{ ML GaSb}$ were grown by MBE, where $X/Y = 14/7, 14/4, 12/4, 10/4$. PL measurements were also performed and verified the predictions of the k.p simulations. Comparing the electrical performance of a 14/7 and 12/4 T2SL as a function of temperature highlights that, although G-R current is lower for the 14/7 T2SL, diffusion current is lower for the 12/4 T2SL, as predicted by k.p simulations and diode theory. This suggests that by using the novel 12/4 T2SL absorption region as part of a barrier detector architecture, which effectively eliminates G-R current, better device performance can be achieved. The k.p simulations also predict further improvements could be achieved by using structures such as the 12/2 T2SL which have not yet been tested experimentally.

5. Conclusion

The T2SL is considered an attractive alternative to current MCT, HOT LWIR detectors due to its numerous theoretical and fabrication advantages. The unique bandgap tunability of the T2SL materials spanning from the SWIR to (V)LWIR has enabled the incorporation of unipolar barriers to eliminate G-R currents. This, in combination with suppressed Auger recombination and tunneling currents, has led to sustained research interest in this material system over the past several decades. System and production advantages such as material robustness, uniformity, manufacturability, and high yield also make this material system more desirable than MCT for FPA applications. Despite numerous theoretical predictions, the performance of T2SL detectors is yet to surpass MCT. The performance limits of LWIR T2SL detectors arise from

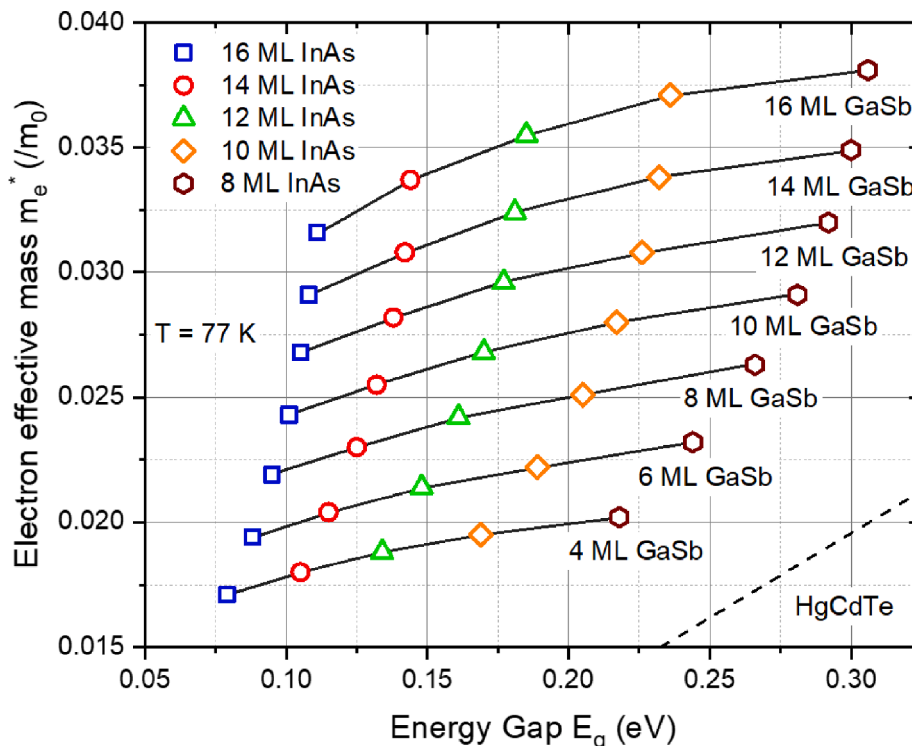


Fig. 9. Electron effective mass and energy bandgap for selected superlattice structures at 77 K.

the fundamental properties of the material system, namely the minority carrier lifetime and minority carrier diffusion length. These parameters directly impact the performance of T2SL detectors via the diffusion and generation-recombination currents.

In this paper, the physics that determines these critical parameters in T2SLs has been examined. Contrary to commonly held assumptions, it is argued that these limiting factors do not necessarily become increasingly restricting as temperature increases. Furthermore, quantum efficiencies comparable to MCT can be achieved by growing thicker active regions in T2SL devices. Further experimental studies are undoubtedly required to demonstrate this capability.

This paper also outlines many recent developments towards achieving T2SL-based HOT LWIR detectors by the mitigation of well-known sources of dark current including BIRDS, CIDs, resonator pixels and the GaAs immersion lens. All these innovations have shown demonstrable improvements over conventional detector designs. Furthermore, many of the techniques described above have the potential to be used in tandem thus compounding the performance benefits. The continued performance improvements, combined with the evidence of material studies, suggest that the T2SL is a competitive material system for achieving high performance, HOT LWIR detectors.

Declaration of Competing Interest

The authors declare that they have no known competing financial interests or personal relationships that could have appeared to influence the work reported in this paper.

References

- [1] G.A. Sai-Halasz, R. Tsu, L. Esaki, *Appl. Phys. Lett.* 30 (1977) 651, <https://doi.org/10.1063/1.89273>.
- [2] M. Razeghi, B.M. Nguyen, *Phys. Procedia* 3 (2010) 1207, <https://doi.org/10.1016/j.phpro.2010.01.164>.
- [3] D.L. Smith, C. Mailhot, *J. Appl. Phys.* 62 (1987) 2545, <https://doi.org/10.1063/1.339468>.
- [4] E.R. Youngdale, J.R. Meyer, C.A. Hoffman, F.J. Bartoli, C.H. Grein, P.M. Young, *Appl. Phys. Lett.* 64 (1994) 3160, <https://doi.org/10.1063/1.111325>.
- [5] C.H. Grein, P.M. Young, M.E. Flatté, H. Ehrenreich, *J. Appl. Phys.* 78 (1995) 7143, <https://doi.org/10.1063/1.360422>.
- [6] G.A. Sai-Halasz, L. Esaki, W.A. Harrison, *Phys. Rev. B* 18 (1978) 2812, <https://doi.org/10.1103/PhysRevB.18.2812>.
- [7] R.N. Nucho, A. Madhukar, *J. Vac. Sci. Technol.* 15 (1978) 1530, <https://doi.org/10.1116/1.569782>.
- [8] J. L. Johnson, L. A. Samoska, A. C. Gossard, J. L. Merz, M. D. Jack, G. R. Chapman B. A. Baumgratz, K. Kosai, S. M. Johnson, 1996 *J. Appl. Phys.* 80 1116 <https://doi.org/10.1063/1.362849>.
- [9] H. Mohseni, E. Michel, J. Sandoen, M. Razeghi, W. Mitchell, G. Brown, *Appl. Phys. Lett.* 71 (1997) 1403, <https://doi.org/10.1063/1.119906>.
- [10] F. Fuchs, U. Weimer, W. Fletschen, J. Schmitz, E. Ahlswede, M. Walther, J. Wagner, P. Koidl, *Appl. Phys. Lett.* 71 (1997) 3251, <https://doi.org/10.1063/1.120551>.
- [11] W. A. Cabanski, K. Eberhardt, W. Rode, J. C. Wendler, J. Ziegler, J. Fleissner, F. Fuchs, R. H. Rehm, J. Schmitz, H. Schneider, M. Walther, 2004 in *Infrared Technology and Applications, SPIE Vol. 5406* (Eds: B. F. Andresen, G. F. Fulop). pp. 184. <https://doi.org/10.1117/12.542186>.
- [12] G.C. Osbourn, *J. Vac. Sci. Technol. B. Microelectron. Process. Phenom.* 2 (1983) 176, <https://doi.org/10.1116/1.582772>.
- [13] C.S. Knox, C. Morrison, F. Herling, D.A. Ritchie, O. Newell, M. Myronov, E. H. Linfield, C.H. Marrows, *Semicond. Sci. Technol.* 32 (2017) 104002, <https://doi.org/10.5518/237>.
- [14] M. Korkmaz, B. Arikian, Y.E. Suyolcu, B. Aslan, U. Serincan, *Semicond. Sci. Technol.* 33 (2018) 035002, <https://doi.org/10.1088/1361-6641/aaa7a0>.
- [15] C.M. Ciesla, B.N. Murdin, C.R. Pidgeon, R.A. Stradling, C.C. Phillips, M. Livingstone, I. Galbraith, D.A. Jaroszynski, C.J.G.M. Langerak, P.J.P. Tang, M. J. Pullin, *J. Appl. Phys.* 80 (1996) 2994, <https://doi.org/10.1063/1.363157>.
- [16] M.J. Pullin, H.R. Hardaway, J.D. Heber, C.C. Phillips, W.T. Yuen, R.A. Stradling, P. Moeck, *Appl. Phys. Lett.* 74 (1999) 2384, <https://doi.org/10.1063/1.123859>.
- [17] A. Wilk, M. El Gouzouli, M. El Skouri, P. Christol, P. Grech, A.N. Baranov, A. Joulie, *Appl. Phys. Lett.* 77 (2000) 2298, <https://doi.org/10.1063/1.1317537>.
- [18] Y.H. Zhang, *Appl. Phys. Lett.* 66 (1995) 118, <https://doi.org/10.1063/1.113535>.
- [19] D. Lackner, O.J. Pitts, M. Steger, A. Yang, M.L.W. Thewalt, S.P. Watkins, *Appl. Phys. Lett.* 95 (2009) 081906, <https://doi.org/10.1063/1.3216041>.
- [20] E.H. Steenbergen, B.C. Connelly, G.D. Metcalfe, H. Shen, M. Wraback, D. Lubyshev, Y. Qiu, J.M. Fastenau, A.W.K. Liu, S. Elhamri, O.O. Celtek, Y. H. Zhang, *Appl. Phys. Lett.* 99 (2011) 251110, <https://doi.org/10.1063/1.3671398>.
- [21] E.H. Steenbergen, Y. Huang, J.H. Ryou, L. Ouyang, J.J. Li, D.J. Smith, R. D. Dupuis, Y.H. Zhang, *Appl. Phys. Lett.* 99 (2011) 071111, <https://doi.org/10.1063/1.3625429>.
- [22] Y. Huang, J. H. Ryou, R. D. Dupuis, V. R. D'costa, E. H. Steenbergen, J. Fan, Y. H. Zhang, A. Petschke, M. Mandl, S. L. Chuang, 2011 *J. Cryst. Growth*. 314 92 <https://doi.org/10.1016/j.jcrysgro.2010.11.003>.
- [23] D. Zuo, R. Liu, D. Wasserman, J. Mabon, Z.Y. He, S. Liu, Y.H. Zhang, E.A. Kadlec, B.V. Olsen, E.A. Shaner, *Appl. Phys. Lett.* 106 (2015) 071107, <https://doi.org/10.1063/1.4913312>.
- [24] A.D. Prins, M.K. Lewis, Z.L. Bushell, S.J. Sweeney, S. Liu, Y.H. Zhang, *Appl. Phys. Lett.* 106 (2015) 171111, <https://doi.org/10.1063/1.4919549>.
- [25] H.S. Kim, O.O. Celtek, Z.Y. Lin, Z.Y. He, X.H. Zhao, S. Liu, H. Li, Y.H. Zhang, *Appl. Phys. Lett.* 101 (2012) 161114, <https://doi.org/10.1063/1.4760260>.
- [26] A. Haddadi, G. Chen, R. Chevallier, A.M. Hoang, M. Razeghi, *Appl. Phys. Lett.* 105 (2014) 121104, <https://doi.org/10.1063/1.4896271>.
- [27] A. Haddadi, A. Dehzangi, S. Adhikary, R. Chevallier, M. Razeghi, 2017 *A. P. L. Mater.* 5 035502 <https://doi.org/10.1063/1.4975619>.
- [28] A.M. Hoang, G. Chen, R. Chevallier, A. Haddadi, M. Razeghi, *Appl. Phys. Lett.* 104 (2014) 251105, <https://doi.org/10.1063/1.4884947>.
- [29] D.Z. Ting, A. Soibel, S.D. Gunapala, *Appl. Phys. Lett.* 108 (2016), 183504, <https://doi.org/10.1063/1.4948387>.
- [30] S. Gunapala, D. Ting, A. Soibel, A. Khoshakhlagh, S. Rafol, C. Hill, A. Fisher, B. Pepper, K. K. Choi, A. D'Souza, C. Masterjohn, S. Babu, P. Ghuman, 2019 in *International Conference on Space Optics — ICSSO. SPIE Vol. 11180* (Eds: N. Karafolas, A. Sodnik, B. Cugny) pp. 136 doi: 10.1117/12.2536056.
- [31] D. Z. Ting, S. D. Gunapala, A. Soibel, A. Khoshakhlagh, S. A. Keo, S. B. Rafol, E. M. Luong, A. M. Fisher, B. J. Pepper, C. J. Hill, 2019 in *IEEE Photonics Conference*, pp. 1 10.1109/IPCCon.2019.8908367.
- [32] P. Tang, M. J. Pullin, S. J. Chung, C. C. Phillips, R. A. Stradling, A. G. Norman, Y. B. Li, L. Mart, 1995 *Semicond. Sci. Technol.* 10 1177 <https://doi.org/10.1088/0268-1242/10/8/023>.
- [33] K. Michalczewski, L. Kubiszyn, P. Martyniuk, C.H. Wu, J. Jureńczyk, K. Grodecki, D. Benyahia, A. Rogalski, J. Piotrowski, *Infrared Phys. Technol.* 95 (2018) 222, <https://doi.org/10.1016/j.infrared.2018.10.024>.
- [34] D.E. Sidor, G.R. Savich, G.W. Wicks, *J. Electron. Mater.* 45 (2016) 4663, <https://doi.org/10.1007/s11664-016-4451-3>.
- [35] D.H. Wu, A. Dehzangi, Y.Y. Zhang, M. Razeghi, *Appl. Phys. Lett.* 112 (2018) 241103, <https://doi.org/10.1063/1.5035308>.
- [36] A. Rogalski, M. Kopytko, M. Piotr, *SPIE Press Book Ch. 1* (2018).
- [37] V. Gopal, S. Gupta, R.K. Bhan, R. Pal, P.K. Chaudhary, V. Kumar, *Infrared, Phys. Technol.* 44 (2003) 143, [https://doi.org/10.1016/S1350-4495\(02\)00185-8](https://doi.org/10.1016/S1350-4495(02)00185-8).
- [38] V. Gopal, E. Plis, J.B. Rodriguez, C.E. Jones, L. Faraone, S. Krishna, *J. Appl. Phys.* 104 (2008) 124506, <https://doi.org/10.1063/1.3042232>.
- [39] V. Gopal, N. Gautam, E. Plis, S. Krishna, *AIP Adv.* 5 (2015) 097132, <https://doi.org/10.1063/1.4930978>.
- [40] W.E. Tennant, *J. Electron. Mater.* 39 (2010) 1030, <https://doi.org/10.1007/s11664-010-1084-9>.
- [41] B-M. Nguyen, D. Hoffman, E. K-W. Huang, P-Y. Delaunay, M. Razeghi, 2008 *Appl. Phys. Lett.* 93 123502 <https://doi.org/10.1063/1.2978330>.
- [42] P.C. Klipstein, E. Avnon, D. Azulai, Y. Benny, R. Fraenkel, A. Glozman, E. Hojman, O. Klin, L. Krasovitsky, L. Langof, I. Shtrichman, N. Rappaport, N. Snapi, E. Weiss, A. Tuito, *Proc SPIE Infrared Technology and Applications* 9819 (2016) 98190T, <https://doi.org/10.1117/12.222776>.
- [43] D.Z.-Y. Ting, C.J. Hill, A. Soibel, S.A. Keo, J.M. Mumolo, J. Nguyen, S. D. Gunapala, *Appl. Phys. Lett.* 95 (2009) 023508, <https://doi.org/10.1063/1.3177333>.
- [44] S. Gunapala, S. Rafol, D. Ting, A. Soibel, A. Khoshakhlagh, S. Keo, B. Pepper, A. Fisher, C. Hill, K-K Choi, A. D'Souza, C. Masterjohn, S. R. Babu, P. Ghuman, 2019 in *Proc. SPIE. Sensors, Systems, and Next-Generation Satellites Vol. 11151* pp. 1115110 <https://doi.org/10.1117/12.2527731>.
- [45] M. Huang, J. Chen, Z. Xu, J. Xu, Z. Bai, F. Wang, Y. Zhou, A. Huang, R. Ding, L. He, *IEEE Photon. Technol. Lett.* 32 (2020) 453, <https://doi.org/10.1109/LPT.2020.2973204>.
- [46] P. Christol, R. Alchaar, J.B. Rodriguez, L. Hoeglund, S. Naureen, R. Marcks von Wurtemberg, C. Asplund, E. Costard, A. Rouvie, J. Brocal, O. Saint-Pe, *Proc SPIE International Conference on Space Optics 11180* (2019) 111806N, <https://doi.org/10.1117/12.2536158>.
- [47] R. Alchaar, J.B. Rodriguez, L. Hoeglund, S. Naureen, P. Christol, *AIP Adv.* 9 (2019), 055012, <https://doi.org/10.1063/1.5094703>.
- [48] L. Hoeglund, C. Asplund, R. Marcks von Wurtemberg, A. Gamfeldt, H. Kataria, D. Lantz, S. Smuk, E. Costard, H. Martijn, in *Proc. SPIE Infrared Technology and Applications Vol. 9819* pp. 98190Z <https://doi.org/10.1117/12.2227466>.
- [49] R. Ivanov, L. Hoeglund, D. Ramos, S. Naureen, M. Pozzi, S. Almgvist, S. Becanovic, D. Rihtnesberg, P. Tinghag, A. Smuk, S. Fattala, S. Smuk, M. Delmas, E. Costard, in *Proc. SPIE Sensors, Systems, and Next-Generation Satellites Vol. 11151* pp. 1115111 <https://doi.org/10.1117/12.2533247>.
- [50] M. Delmas, D.C.M. Kwan, M.C. Debnath, B.L. Liang, D. L. Huffaker, *J. Phys. D Appl. Phys.* 52 475102 <https://doi.org/10.1088/1361-6463/ab3b6a>.
- [51] P.C. Klipstein, Y. Benny, S. Gliksman, A. Glozman, E. Hojman, O. Klin, *Infrared, Phys. Technol.* 96 (2019) 155, <https://doi.org/10.1016/j.infrared.2018.11.022>.
- [52] J.W. Matthews, A.E. Blakeslee, *J. Cryst. Growth* 27 (1974) 118, [https://doi.org/10.1016/S0022-0248\(74\)80055-2](https://doi.org/10.1016/S0022-0248(74)80055-2).
- [53] L. Hoeglund, J.B. Rodriguez, R. Marcks von Wurtemberg, S. Naureen, R. Ivanov, C. Asplund, R. Alchaar, P. Christol, A. Rouvie, O. Saint-Pe, E. Costard, *Infrared Phys. Technol.* 95 (2018) 158, <https://doi.org/10.1016/j.infrared.2018.10.036>.

- [54] P.C. Klipstein, E. Avnon, Y. Benny, Y. Cohen, R. Fraenkel, S. Gliksman, A. Glozman, E. Hojman, O. Klin, L. Krasovitsky, L. Langof, I. Lukomsky, I. Marderfeld, N. Yaron, M. Rappaport, I. Shtrichman, N. Snapi, E. Weiss, *J. Electron. Mater.* 47 (2018) 5725, <https://doi.org/10.1007/s11664-018-6527-8>.
- [55] S. Hanna, A. Bauer, H. Bitterlich, D. Eich, M. Finck, H. Figgemeier, W. Gross, K. M. Mahlein, A. Wegmann, *J. Electron. Mater.* 49 (2019) 6946, <https://doi.org/10.1007/s11664-020-08224-5>.
- [56] H. Haiml, D. Eich, W. Fick, H. Figgemeier, *Proc SPIE International Conference on Space Optics 10562* (2019) 1056262, <https://doi.org/10.1117/12.2552098>.
- [57] H. Lutz, R. Breiter, D. Eich, H. Figgemeier, S. Hanna, *Proc SPIE Infrared Technology and Applications 11002* (2019) 1100216, <https://doi.org/10.1117/12.2519811>.
- [58] B. Asici, A. San, B. Barutcu, H. Cuneit Eroglu, A. Tolunguc, C. Ozgit-Akgun, U. Tumkaya, R. Kepenek, C. Tunca, M. Akbulut, O. Lutfi Nuzumlali, E. Inceurkmen, *Proc SPIE Infrared Technology Applications 11002* (2019) 110021A, <https://doi.org/10.1117/12.2518867>.
- [59] A. Rogalski, P. Martyniuk, M. Kopytko, *Appl. Phys. Rev.* 4 (2017) 031304, <https://doi.org/10.1063/1.4999077>.
- [60] Z. Taghipour, S. Lee, S.A. Myers, E.H. Steenbergen, C.P. Morath, V.M. Cowan, S. Mathews, G. Balakrishnan, S. Krishna, *Phys. Rev. Appl.* 11 (2019) 024047, <https://doi.org/10.1103/PhysRevApplied.11.024047>.
- [61] B.C. Connelly, G.D. Metcalfe, H. Shen, M. Wraback, C.L. Canedy, I. Vurgaftman, J. S. Melinger, C.A. Affouda, E.M. Jackson, J.A. Nolde, J.R. Meyer, E.H. Aifer, *J. Electron. Mater.* 42 (2013) 3203, <https://doi.org/10.1007/s11664-013-2759-9>.
- [62] D. Donetsky, S.P. Svensson, L.E. Vorobjev, G. Belenky, *Appl. Phys. Lett.* 95 (2009) 212104, <https://doi.org/10.1063/1.3267103>.
- [63] D. Donetsky, G. Belenky, S. Svensson, S. Suchalkin, *Appl. Phys. Lett.* 97 (2010) 052108, <https://doi.org/10.1063/1.3476352>.
- [64] G. Belenky, G. Kipshidze, D. Donetsky, S.P. Svensson, W.L. Sarney, H. Hier, L. Shterengas, D. Wang, Y. Lin, *Proc SPIE Infrared Technology and Applications 8012* (2011) 80120W, <https://doi.org/10.1117/12.883625>.
- [65] B.C. Connelly, G.D. Metcalfe, H. Shen, M. Wraback, *Appl. Phys. Lett.* 97 (2010) 251117, <https://doi.org/10.1063/1.3529458>.
- [66] L. Hoeglund, A. Soibel, D.Z. Ting, A. Khoshakhlagh, C.J. Hill, S.D. Gunapala, *Proc SPIE Infrared Remote Sensing and Instrumentation 8511* (2013) 851106, <https://doi.org/10.1117/12.930136>.
- [67] L. Hoeglund, D.Z. Ting, A. Khoshakhlagh, A. Soibel, C.J. Hill, A. Fisher, S. Keo, S. D. Gunapala, *Appl. Phys. Lett.* 103 (2013) 221908, <https://doi.org/10.1063/1.4835055>.
- [68] B.V. Olson, C.H. Grein, J.K. Kim, E.A. Kadlec, J.F. Klem, S.D. Hawkins, E. A. Shaner, *Appl. Phys. Lett.* 107 (2015) 261104, <https://doi.org/10.1063/1.4939147>.
- [69] Y. Aytac, B.V. Olson, J.K. Kim, E.A. Shaner, S.D. Hawkins, J.F. Klem, M.E. Flatte, T.F. Boggess, *Appl. Phys. Lett.* 105 (2014) 022107, <https://doi.org/10.1063/1.4890578>.
- [70] J. Pellegrino, R. DeWames, 2009 *Proc. in SPIE Infrared Technology and Applications 7298* 72981U <https://doi.org/10.1117/12.819641>.
- [71] M.A. Kinch, F. Aqariden, D. Chandra, P.-K. Liao, H.F. Schaake, H.D. Shih, *J. Electron. Mater.* 34 (2005) 880, <https://doi.org/10.1007/s11664-005-0036-2>.
- [72] S. Krishnamurthy, N.T. Casselman, *J. Electron. Mater.* 29 (2000) 828, <https://doi.org/10.1007/s11664-000-0232-z>.
- [73] A. Rogalski, P. Martyniuk, M. Kopytko, *Prog. Quantum Electron.* 68 (2019) 100228, <https://doi.org/10.1016/j.pquantelec.2019.100228>.
- [74] P.C. Klipstein, Y. Benny, Y. Cohen, N. Fraenkel, S. Gliksman, A. Glozman, *J. Electron. Mater.* 49 (2020) 1, <https://doi.org/10.1007/s11664-020-08195-7>.
- [75] Y. Aytac, B.V. Olson, J.K. Kim, E.A. Shaner, S.D. Hawkins, J.F. Klem, M.E. Flatte, T.F. Boggess, *J. Appl. Phys.* 118 (2015) 125701, <https://doi.org/10.1063/1.4953386>.
- [76] S. Maimon, G.W. Wicks, *Appl. Phys. Lett.* 89 (2006) 151109, <https://doi.org/10.1063/1.2360235>.
- [77] A. Khoshakhlagh, S. Myers, H. Kim, E. Plis, N. Gautam, S.J. Lee, S.K. Noh, L. R. Dawson, S. Krishna, *IEEE J. Quantum Electron.* 46 (2010) 959, <https://doi.org/10.1109/JQE.2010.2041635>.
- [78] P. C. Klipstein, E. Avnon, Y. Benny, R. Fraenkel, A. Glozman, S. Grossman, O. Klin, L. Langoff, Y. Livneh, I. Lukomsky, M. Nitzani, L. Shkedy, I. Schtrichman, N. Snapi, A. Tuito, E. Weiss, 2014 in *Infrared Technology and Applications - Proc. SPIE*. pp. 90700U <https://doi.org/10.1117/12.2049825>.
- [79] A.D. Hood, A.J. Evans, A. Ikhlasi, D.L. Lee, W.E. Tennant, *J. Electron. Mater.* 39 (2010) 1001, <https://doi.org/10.1007/s11664-010-1091-x>.
- [80] B-M. Nguyen, D. Hoffman, P-Y Delaunay, E. K. Huang, M. Razeghi, 2008 in *Infrared Spaceborne Remote Sensing and Instrumentation XVI - Proc. SPIE*. pp. 708205 doi: 10.1117/12.794210.
- [81] N. Gautam, H.S. Kim, M.N. Kutty, E. Plis, L.R. Dawson, S. Krishna, *Appl. Phys. Lett.* 96 (2010) 231107, <https://doi.org/10.1063/1.3446967>.
- [82] R.T. Hinkey, R.Q. Yang, *J. Appl. Phys.* 114 (2013) 10450, <https://doi.org/10.1063/1.4820394>.
- [83] L. Lei, L. Lu, H. Ye, H. Lotfi, R.Q. Yang, M.B. Johnson, J.A. Massengale, T. D. Mishima, M.B. Santos, *J. Appl. Phys.* 120 (2016) 193102, <https://doi.org/10.1063/1.4967915>.
- [84] K. Hackiewicz, J. Rutkowski, P. Martyniuk, *IEEE J. Quantum Electron.* 55 (2019) 1, <https://doi.org/10.1109/JQE.2019.2923910>.
- [85] E.K.W. Huang, D. Hoffman, B.M. Nguyen, P.Y. Delaunay, M. Razeghi, *Appl. Phys. Lett.* 94 (2009) 053506, <https://doi.org/10.1063/1.3254719>.
- [86] H.S. Kim, E. Plis, N. Gautam, S. Myers, Y. Sharma, L.R. Dawson, S. Krishna, *Appl. Phys. Lett.* 97 (2010) 143512, <https://doi.org/10.1063/1.3499290>.
- [87] T. Specht, S. Myers, T. J. Ronningen, A. Kazemi, D. Hollingshead, E. Fuller, S. Krishna, 2018 in *IEEE Research and Applications of Photonics In Defense Conference (RAPID)*. pp. 22 10.1109/RAPID.2018.8508916.
- [88] O. Salihoglu, A. Muti, A. Aydinli, *IEEE J. Quantum Electron.* 49 (2013) 661, <https://doi.org/10.1109/JQE.2013.2267553>.
- [89] O. Salihoglu, A. Muti, K. Kuttler, T. Tansel, R. Turan, C. Kocabas, A. Aydinli, *J. Appl. Phys.* 111 (2012) 074509, <https://doi.org/10.1063/1.3702567>.
- [90] R. Rehm, M. Walther, F. Fuchs, J. Schmitz, J. Fleissner, *Appl. Phys. Lett.* 86 (2005) 1, <https://doi.org/10.1063/1.1906326>.
- [91] E. Plis, M. N. Kutty, S. Myers, S. Krishna, C. Chen, J. D. Phillips, 2014 in *Infrared Technology and Applications - Proc. SPIE*. pp. 907010 <https://doi.org/10.1117/12.2050490>.
- [92] N.C. Henry, A. Brown, D.B. Knorr, N. Baril, E. Nallon, J.L. Lenhart, M. Tidrow, S. Bandara, *Appl. Phys. Lett.* 108 (2016) 011606, <https://doi.org/10.1063/1.4938168>.
- [93] J.A. Nolde, E.M. Jackson, M.F. Bennett, C.A. Affouda, E.R. Cleveland, C. L. Canedy, I. Vurgaftman, G.C. Jernigan, J.R. Meyer, E.H. Aifer, *Appl. Phys. Lett.* 111 (2017) 051102, <https://doi.org/10.1063/1.4997172>.
- [94] E.H. Aifer, J.H. Warner, C.L. Canedy, I. Vurgaftman, E.M. Jackson, J.G. Tischler, J.R. Meyer, S.P. Powell, K. Olver, W.E. Tennant, *J. Electron. Mater.* 39 (2010) 1070, <https://doi.org/10.1007/s11664-009-1056-0>.
- [95] G. Chen, B.M. Nguyen, A.M. Hoang, E.K. Huang, S.R. Darvish, M. Razeghi, *Appl. Phys. Lett.* 99 (2011) 183503, <https://doi.org/10.1063/1.3658627>.
- [96] G. Chen, E.K. Huang, A.M. Hoang, S. Bogdanov, S.R. Darvish, M. Razeghi, *Appl. Phys. Lett.* 101 (2012) 213501, <https://doi.org/10.1063/1.4767905>.
- [97] G. Chen, A.M. Hoang, S. Bogdanov, A. Haddadi, S.R. Darvish, M. Razeghi, *Appl. Phys. Lett.* 103 (2013) 223501, <https://doi.org/10.1063/1.4833026>.
- [98] G. Chen, A.M. Hoang, M. Razeghi, *Appl. Phys. Lett.* 104 (2014) 103509, <https://doi.org/10.1063/1.4868486>.
- [99] H.S. Kim, S. Myers, B. Klein, A. Kazemi, S. Krishna, J.O. Kim, S.J. Lee, J. Korean. Phys. Soc. 66 (2015) 535, <https://doi.org/10.3938/jkps.66.535>.
- [100] J. Piotrowski, W. Galus, M. Grudzien, *Infrared Physics*. Pergamon. 31 (1991) 48, [https://doi.org/10.1016/0020-0891\(91\)90037-G](https://doi.org/10.1016/0020-0891(91)90037-G).
- [101] J. Piotrowski, A. Rogalski, *Infrared Phys. Technol.* 46 (2004) 115, <https://doi.org/10.1016/j.infrared.2004.03.016>.
- [102] K. Michalczewski, P. Martyniuk, L. Kubiszyn, C.-H. Wu, Y.-R. Wu, J. Jureczyk, A. Rogalski, J. Piotrowski, *IEEE Electron Device Lett.* 40 (2019) 1396, <https://doi.org/10.1109/LED.2019.2930106>.
- [103] R. Müller, V. Gramich, M. Wauro, J. Niemasz, L. Kirste, V. Daumer, A. Janaszek, J. Jureczyk, R. Rehm, *Infrared Phys. Technol.* 96 (2019) 141, <https://doi.org/10.1016/j.infrared.2018.10.019>.
- [104] S. Huang, G. Balakrishnan, D.L. Huffaker, *J. Appl. Phys.* 105 103104 (2009), <https://doi.org/10.1063/1.3129562>.
- [105] D. Benyahia, K. Kubiszyn, J. Michalczewski, A. Boguski, P. Kęblowski, J. Martyniuk, A. Rogalski Piotrowski, *Nanoscale, Res. Lett.* 13 (2018) 196, <https://doi.org/10.1186/s11671-018-2612-4>.
- [106] K. Michalczewski, T.Y. Tsai, P. Martyniuk, C. H. Wu. 2019 *Bull. Polish. Acad. Sci. Tech. Sci.* 67 141 DOI: 10.24425/bpas.2019.127343.



Dominic Kwan is a PhD student in the physics department of Cardiff University under the supervision of Dr. Manoj Kesaria and Prof. Diana Huffaker. His research focuses on developing LWIR InAs/GaSb T2SL photodetectors primarily through enhanced fabrication methods, characterization and simulation. He has a particular interest in the LWIR T2SLs on GaAs substrates using the interfacial misfit array and the development of novel SL structures for high-performance LWIR applications. He has a bachelor's degree in physics and a master's degree in nanotechnology, both from Swansea University.



Dr Manoj Kesaria received the PhD degree in 2012 from Jawaharlal Nehru Centre for Advanced Scientific Research (JNCASR), Bangalore, India. Between 2012-18, he has worked as a research scientist and senior research associates at the Universities of Houston, Lancaster, and Sheffield. He is currently a Lecturer/Assistant Professor at the School of Physics and Astronomy at Cardiff University (CU). He is presently involved in the development of novel III-V (Nitride, Arsenide and Antimonides) compound semiconductor epitaxy, design, simulation fabrication, and characterisation of infrared (SWIR to LWIR), detectors, Light-emitting diodes (LED) and Thermophotovoltaics (TPV).



Prof. Diana L. Huffaker (FIEEE, FOSA, FLSW) was the Welsh Government Sêr Cymru Chair in Advanced Materials and Engineering. She was Science Director for the Institute for Compound Semiconductors (ICS) with considerable experience in managing large, multi-institutional programmes supported by the US National Science Foundation, Department of Defence etc. Since Aug. 2020, She is chair of the Electrical Engineering Department at UT Arlington. She is a pioneer in MBE growth of III-Sb bulk and quantum dot materials and recently demonstrated growth of Sb material using the DA technique. Her research expertise includes novel III-As,Sb epitaxial methods, fabrication and high performance detectors.